AIAA 79-1517R

Iterative Lifting Surface Method for Thick Bladed Hovering Helicopter Rotors

K. Rajarama Shenoy* and Robin B. Gray†
Georgia Institute of Technology, Atlanta, Ga.

A prescribed-wake, inviscid, incompressible, lifting-surface method using vortex sheets to define the upper and lower blade surfaces is developed to predict the pressure distribution on helicopter blades in hover. Starting with an approximate upper and lower surface vortex sheet strength distribution obtained by using a lifting-line/blade-element method, the final strength distribution is computed iteratively by applying the Biot-Savart law. The convergence rate is rapid and reasonably good results can be obtained within three iterations. The method is used to compute the blade pressure distribution in hover for a single-bladed, teetering model helicopter rotor with negligible blade coning. The constant-chord, untwisted blade has a body of revolution tip and is structurally rigid. The results show good agreement with experimental data except very near the blade tip in the trailing-edge region of the upper surface where the effects of the formation of the tip vortex predominate. At spanwise stations inboard of the maximum blade bound circulation, the iterative procedure produces only small changes in the initial two-dimensional blade-element pressure distributions.

Nomenclature

A = tip vortex contraction ratio
b = number of blades
B = nondimensional point of origin of tip vortex
c = blade chord
C_p = pressure coefficient, $(p-p_\infty)/\frac{1}{2}\rho\Omega^2 y^2$
k_1 = tip vortex axial displacement parameter, $\psi < 2\pi/b$
k_2 = tip vortex axial displacement parameter, $\psi > 2\pi/b$
p = static pressure
p_∞ = static pressure in undisturbed fluid
r = radial coordinate, Fig. 3
R = tip radius including half-body of revolution
ΔS = vortex sheet element
U = total velocity
U_∞ = effective two-dimensional relative wind at blade element
v = induced velocity vector
x,y = blade coordinates, Fig. 2
Y = tip radius excluding half-body of revolution
z = axial coordinate of tip vortex, Eqs. (6) and (7), and blade coordinate perpendicular to x-y plane, Fig. 2
α = vorticity component in spanwise direction
β = vorticity component in chordwise direction
γ = vortex sheet strength
γ_1 = vortex sheet strength for two-dimensional flow parallel to chordline
γ_2 = vortex sheet strength for two-dimensional flow perpendicular to chordline
θ = blade collective pitch angle
θ_e = effective angle of attack, angle between chordline and relative wind
θ_{eq} = reduced blade collective pitch angle
θ_i = induced angle of attack of blade element
λ = tip vortex contraction parameter
λ_M = tip vortex formation model contraction parameter
ρ = fluid density
χ = blade surface slope parameter, $[1+(dz/dx)^2]^{\frac{1}{2}}$
ψ = azimuth along tip vortex, Fig. 3
ψ_M = azimuth at which tip vortex and formation model meet
ψ_S = azimuth over which tip vortex strength varies
Ω = blade angular velocity

Presented as Paper 79-1517 at the AIAA 12th Fluid and Plasma Dynamics Conference, Williamsburg, Va., July 23-25, 1979; submitted Aug. 2, 1979, revision received Nov. 17, 1980. Copyright © American Institute of Aeronautics and Astronautics, Inc., 1979. All rights reserved.

*Graduate Research Assistant, Aerospace Engineering. Currently, Senior Aerodynamics Engineer, Bell Helicopter Textron, Fort Worth, Texas. Member AIAA.
†Regents' Professor, Aerospace Engineering. Member AIAA.

Introduction

HOVER performance prediction methods have been based on momentum theories[1-3] and vortex-wake theories. The wake models in the vortex theories can be classified as: 1) classical noncontracting wake[4-6]; 2) free wake[6-8]; and 3) prescribed wake.[9-12] Modern-day helicopters with higher disk loadings have considerable wake contraction and the prescribed wake analysis, in which the trailing tip vortex and inner vortex sheet geometries are determined from experiment, has taken precedence over the ones using the classical wake. The free wake analysis is computationally demanding and does not yield the correct tip vortex geometry but a modification, when used in conjunction with a prescribed tip vortex geometry, will yield reasonably good inner sheet geometries. Consequently, the prescribed wake analysis with a free wake procedure for determining the inner sheet geometries has been shown to yield improved predictions of hover performance and therefore represents the current state of the art.

The validity of the prescribed wake analysis with a lifting-line/blade-element representation for the blade appears to have been first demonstrated in Ref. 9 and Landgrebe[11] extended this method to cover a wide range of rotor systems. Kucurek and Tangler[12] have used a thin lifting surface representation for the blade with prescribed tip vortex geometries, a recirculating wake model, and computed inner vortex sheet geometries. Although these approaches appear to be valid over most of the blade, they are not appropriate near the blade tip. Unlike conventional wings, the tip region of the helicopter rotor blade is relatively more important since the largest dynamic pressures occur there. In addition, pressure measurements[13,14] on a blade tip show a rearward shift in the center of pressure with a significant increase in pressure drag. Thus, more accurate flow prediction methods are necessary for the tip region.

The problem may be defined and a solution may be found in terms of either the velocity potential or the application of the Biot-Savart law to distributed vortex sheets and filaments. In principle, the two approaches are similar and should yield comparable results for comparable numerical solution

techniques in fluid mediums which are incompressible or compressible (nonlinear or linear with retarded time concepts, as appropriate).

An example of the perturbation velocity potential and its application to horizontal axis windmills is given in Ref. 15 along with several examples for hovering helicopter rotors. Reference 15 uses the classical Green's function approach and formulates the analysis for both finite-thickness and zero-thickness blades. Blade loading distributions for each formulation using a classical wake are given for a single-bladed hovering rotor. There are only small differences shown between the distributions, even very near the blade tip. Thus, these results indicate that the blade thickness has very little effect on the load distribution. A comparison between the results of the zero-thickness formulation method and experimental results are also presented for a four-bladed hovering rotor. The comparison shows appreciable differences particularly near the tip. This is attributed to the use of the classical wake instead of the prescribed wake for determining the inflow distribution. Reference 16 gives a Green's function method for the computational aerodynamic analysis of complex helicopter configurations which includes thick blades. The computed spanwise loadings are shown to be appreciably different from those of Ref. 15 for the single-bladed hovering rotor which may indicate significant, but not obvious, differences in procedure. Likewise, the comparison with experiment for the four-bladed hovering rotor is much better except, again, near the tip because a classical wake was used in the computations. Neither reference presents chordwise pressure distributions so that no data of this kind are available for comparison with the results of this paper.

For flow problems such as the hovering rotor in which the vortex sheet and filament geometries cannot be specified in advance, the Biot-Savart law approach offers a direct advantage in that the procedure can be set up to iterate on the velocity field to find a converged vortex geometry which is consistent with the Helmholtz theorems. On the other hand, in a similar procedure using the velocity potential, a separate calculation for the velocity field must be performed in each iteration. Therefore, since the approach using the Biot-Savart law offers some advantage and since vortex sheets and filaments provide a more realistic modeling of physical boundary layers and wakes, the authors of this paper have chosen to take this approach.

Although the lifting-line/blade-element/prescribed-wake analysis has demonstrated improved hovering performance predictions, it is incomplete in two important aspects which have also impeded the development of a completely theoretical analysis. One of these deficiencies is represented by the lack of a method for computing the tip vortex geometry so that this geometry must be determined from observations. A discussion of this problem and a suggested method for reducing the number of empirical parameters is given in Ref. 17. A second deficiency is that this simplified model of the rotor cannot account for the effect of tip shape on performance. It is expected that a thick-blade formulation would be necessary to include this effect but this, in turn, would require a modeling of the tip vortex formation and shedding mechanism. To the authors' knowledge, a satisfactory model of this phenomenon has not been developed.

The necessity for defining an accurate tip-vortex geometry in the near wake has been well documented (for example, Refs. 18 and 19). Reference 18 also demonstrates that although different wake modeling procedures can yield nearly identical integrated thrusts, the spanwise blade angle-of-attack distribution can be appreciably different. The authors of that reference contend that the lifting line approach is adequate for predicting the hover performance of a wide range of conventional and advanced rotors and question whether a zero-thickness, lifting-surface analysis[12] represents a justified improvement from a computer cost viewpoint. They do, however, recognize that a lifting surface representation of the blade may be required for advanced rotors with complex tip designs. On the other hand, the authors of Ref. 19 contend that their lifting surface theory is required for more accurate calculation of radial load distribution and correct calculation of rotor induced torque. The comparisons of their computed performance with test data for 19 rotor systems is impressive since the error band is plus or minus 3%. Since the method of Ref. 18 used a truncated wake and the method of Ref. 19 uses a recirculation wake, the predicted blade load distributions are significantly different. Although the authors of both references disagree as to the suitability of the others' approach, they do agree that additional work needs to be done.

The data of Ref. 14 indicate that there appear to be two primary effects that influence the loading in the blade-tip region. One of these is a three-dimensional tip relief and the other is due to the formation and growth of the tip vortex as it sweeps rearward over the upper surface of the blade. The tip relief effect is most predominant outboard of $y/Y=0.94$ and the tip vortex effect is most predominant outboard of $y/Y=0.98$ and aft of the 50% chord station. Since a method had been developed for computing the three-dimensional tip relief effect on nonlifting wings,[20] an investigation was undertaken to adapt that method to rotor blades and to attempt to separate the tip vortex effect from the other effects which seemed to be susceptible to reasonably accurate modeling. In this regard, unpublished flow visualization studies which were performed on the model rotor of Ref. 14 indicated that the tip vortex maintained its coherent character for at least eight revolutions and an axial length of one diam. This may be due to some influence from the test facility but is certainly characteristic of single-bladed rotors. Therefore, for the following analysis, the truncated wake of Refs. 9 and 10 is used rather than the recirculation wake of Ref. 12.

The objective of this paper was to develop a numerical method for computing the pressure distribution on a hovering rotor blade, specifically, for comparison with the single-bladed data of Ref. 14. Emphasis was placed on an accurate description of the blade and vortex-wake geometries using proven empirical procedures. No attempt was made to accurately model the tip vortex shedding mechanism. Computing efficiency was a secondary consideration. This work was exploratory in nature and was undertaken in an attempt to isolate specific areas in which additional modeling was needed. Therefore, no effort was directed toward developing a computer code suitable for routine computations. The complete development of the method is given in Ref. 21.

Since the investigation was exploratory, no attempt was made to generalize the analysis to include computational provision for blades of arbitrary planform and airfoil section nor for multibladed rotors. Within the present objectives, the authors did not feel that this was warranted when the investigation was started. However, it was felt that if the approach were successful, then it would be appropriate to extend the analysis to include other blade and rotor geometries and compressible and viscous effects.

Flow Model

The primary interest of this exploratory investigation is on three-dimensional blade tip relief and on the effect on the pressure distribution of the rearward sweep of the tip vortex over the upper surface of the blade tip. The analytical model is simplified to include only those essential elements which in the authors' opinion are consistent with the test models and conditions for which data[9,10,14] are available. Since these data are for low tip speeds as compared to the speed of sound, the assumption of an incompressible fluid medium is reasonable. The assumption of an inviscid fluid medium makes the problem more tractable from both a programing and a computer-cost viewpoint. Thus: boundary-layer effects including centrifugal pumping are neglected; there is no mechanism for vortex shedding or vorticity transport other than in accordance with the Helmholtz vortex theorems; and,

the computed section lift curve slope, unless adjusted, will be much too high. The relevant analytical and numerical relationships[21] are based on the Biot-Savart law and the Helmholtz vortex theorems. The development of these relationships is relatively straightforward but their number and length preclude their inclusion in this paper. Therefore, the following discussion will deal almost entirely with the description of and the rationale leading to the flow model.

If it is assumed that all of the trailing vorticity shed outboard of the point of maximum blade bound circulation rolls up to form the tip vortex, then by the Helmholtz theorems, the tip vortex strength is equal to the maximum blade bound circulation. Therefore, a procedure is required not only to assure that this equality condition is met but to determine a tip vortex strength which is compatible with the measured tip-vortex geometry since the state-of-the-art requires that a prescribed-wake model be used. The problems involved in satisfying these conditions are discussed in Refs. 8 and 17.

As based on Ref. 17, the method used here begins by specifying a thrust coefficient and the corresponding blade collective pitch angle as determined from the test data.[14] The tip-vortex geometric parameters are then obtained from Ref. 9. If an ultimate wake is assumed to exist and its geometry is determined from an extrapolation of the measured parameters, a relationship can be derived[17] for the tip vortex strength. However, this relationship is in error because of the lack of a proper tip-vortex core model and the value computed thereby is useful only as an initial approximation. This approximate value of the tip vortex strength and the Biot-Savart law permit the computation of the induced velocity at the blade lifting line. In this and the following computations, the tip vortex is terminated after twelve revolutions.

Using a lifting-line/blade-element approach and the measured blade collective pitch angle, the value and location of the maximum blade bound circulation are determined. A blade-section lift curve slope is required for this computation and the value selected is that for the two-dimensional airfoil at the blade section Mach and Reynolds numbers as obtained from wind-tunnel tests. The tip-vortex strength is then set equal to the maximum blade bound circulation and the process is repeated until both values are equal. The advantage of this procedure is that it yields a consistent prescribed-wake/lifting-line model; that is, the tip vortex strength is equal to the maximum blade bound circulation and the ultimate wake model satisfies the "free vortex" conditions.[17] Assuming the local applicability of two-dimensional airfoil characteristics, the procedure is restricted by the requirement that both the thrust and the blade collective pitch angle be known. The generalization of this step would appear to await the definition of a more realistic tip-vortex core model.

The next step is to compute the geometry of the trailing vortex sheet that is shed from the blade inboard of the point of maximum blade bound circulation. The smoke studies of Ref. 9 show that the trailing sheet does not roll up in the near wake, that the intersection of the sheet with any azimuthal plane is approximately a straight line, and that the inward extrapolation of this line intersects the axis of rotation at, approximately, the rotor plane. These observations permit the definition of a simple, reasonably accurate sheet geometry which greatly reduces the computational effort. The procedure described below is based on but is not as extensive as that of Ref. 8.

Using the prescribed-wake/lifting-line model, the blade radius is determined at which the local blade bound circulation is computed to be 90% of the maximum value. The outer edge of the inner sheet is then arbitrarily defined as leaving the lifting line at a point midway between this radius and that of the maximum blade bound circulation. Using this midpoint as a base, an axially symmetric, contracting surface is constructed which is concentric with and geometrically similar to the surface along which the tip vortex is prescribed to move. That is, the ratio of the local radii of the two surfaces is the same as that at the blade. The location on this constructed surface of the outer edge of the inner sheet is determined by starting at the previously defined midpoint and integrating the axial component of the induced velocity associated with the tip vortex and the lifting line. The integration is performed in radial planes of 10 deg of azimuthal spacing during 10 deg steps of blade rotation for 4 blade revolutions. The points so determined are connected with straight-line vortex elements which define a continuous filament whose strength is equal to the change in lifting-line strength over the spanwise interval.

The entire trailing sheet is replaced by similar finite-strength filaments of equal strength except for the root filament which accounts for the remainder. The radial locations of these filaments are determined in a similar manner. The axial locations in each radial plane are set by the ratio of the local radius to the outer-edge radius times the local axial location of the outer edge. Thus the intersection points of the inner filaments with each radial plane form straight lines which are approximately in agreement with the results of the smoke studies. Iterations on this entire procedure for the complete wake are performed until converged values are obtained for the trailing sheet geometry and filament strengths, the lifting line circulation distribution with radius, and the maximum blade bound circulation which is also the tip vortex strength. Using these converged values, the computed thrust agrees within 0.5% of the measured values of Ref. 14.

Of the flow characteristics now known, the vortex wake geometry, the maximum blade bound circulation, and the tip vortex strength are held fixed for the thick-blade analysis that follows. Fixing the trailing sheet geometry greatly reduces the computational effort and will probably lead to some error in the computed pressure distributions on the inboard blade elements. However, there should be only a very small effect in the tip regions. The strength distribution of the trailing sheet is, of course, permitted to vary with blade circulation in accordance with the Helmholtz theorem for vortex continuity. The geometry of the analytical model is shown in Fig. 1.

The thick-blade analysis begins by replacing the lifting line with the blade of the test model. The blade has a body-of-revolution tip which eliminates surface discontinuity problems. The NACA 0012 airfoil has a blunt trailing edge so the upper and lower surfaces are extended and the Kutta condition is satisfied at their line of intersection. Thus, in this potential analysis, the chordwise component of velocity relative to the blade is zero at a small distance aft of the trailing edge. This artifice eliminates the computational problems in this area on the physical surface of the airfoil.

A vortex sheet having vorticity components in both the spanwise direction (α vorticity) and the chordwise direction (β vorticity) is superimposed on the blade surfaces. The initial

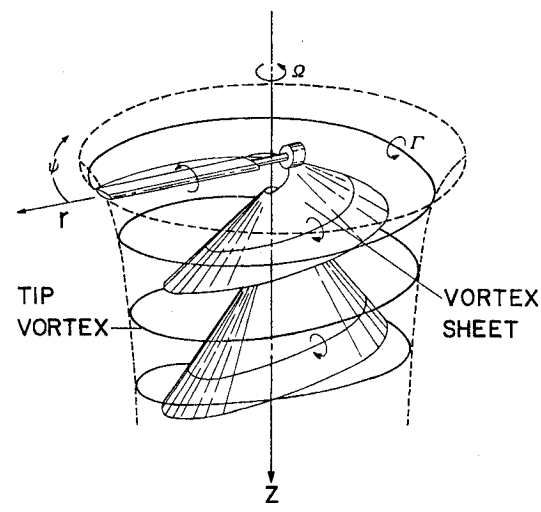

Fig. 1 Schematic diagram of the hovering rotor wake (Ref. 9).

vorticity distribution of the sheet is obtained by two-dimensional potential methods as based on Prandtl's hypothesis for three-dimensional wings. This hypothesis states that the section of the finite wing behaves just as though it were a section of an infinite wing set at an absolute angle of attack equal to the effective angle of attack. Here, the effective angle of attack is defined as the angle between the zero lift line of and the relative wind at the section. Since the induced velocity distribution is known from the lifting line analysis, the effective angle of attack distribution is computed and the chordwise distribution of the two-dimensional spanwise component of the vorticity in the surface sheet is determined using potential methods to satisfy the boundary condition of no flow normal to the surface.

This process is simplified by recognizing that the potential two-dimensional sheet strength can be considered to be composed of two parts. One part is the nonlifting solution, γ_1, obtained for a unit flow parallel to the chordline for symmetrical sections. The second part is the lifting solution, γ_2, obtained for a unit flow perpendicular to the chordline and by forcing a stagnation point at the trailing edge. The advantage of this approach is that the two-dimensional potential solution for any angle of attack may be easily computed by superposition as shown in Eq. (1).

As noted before, the potential solution predicts a lift curve slope which is much too high. For example, the potential-flow slope for the NACA 0012 airfoil is 6.88/rad whereas the measured value at the Reynolds number corresponding to the radius of maximum blade bound circulation is 5.44/rad. The simplest method for correcting for the Reynolds number effect is to reduce the strength of the lifting solution by the ratio of the lift-curve slopes. Thus, at any point on the blade,

$$\alpha/U_\infty = \gamma_1 \cos\theta_e \pm (5.44/6.88)\gamma_2 \sin\theta_e \qquad (1)$$

where θ_e is the effective angle of attack as defined and computed before and the plus sign refers to the upper surface. This relationship implies a reduction in the flow (effective freestream velocity) perpendicular to the chordline or, more consistently, a reduction in the effective angle of attack. For the vortex-sheet-strength redistribution analysis that follows, the adjustment is made to the collective pitch angle to find an equivalent angle,

$$\theta_{eq} = \theta_i + (5.44/6.88)(\theta - \theta_i) \qquad (2)$$

where all of these quantities are determined at the blade radius for the maximum-blade bound circulation. This simple adjustment alters the flow about the leading edge and results in discrepancies in the pressure distribution in this region. However, the results of the redistribution analysis that are to be described show that some compensation of this effect is provided by the procedure, at least in the tip region. The result obtained from Eq. (2) is not changed during the redistribution procedure.

The α vorticity obtained from Eq. (1) varies from point to point as the local boundary conditions change. Therefore to maintain vortex sheet strength continuity according to the Helmholtz theorems, β vorticity must be accounted for in the chordwise direction. For a three-dimensional wing, the necessary relationship is

$$\partial\alpha/\partial y - (1/\chi)\partial\beta/\partial x = 0$$

since the oncoming freestream is irrotational. However, this analysis is performed in a blade-fixed reference so that the oncoming fluid appears to be rotating as a solid body, that is, appears to be a fluid region of uniform vorticity whose direction is parallel to the axis of rotation. This "freestream" vorticity is forced to join with the blade surface vorticity so that the "fluid" within the blade remains irrotational and at rest relative to the blade. Thus for the rotating blade, the continuity condition is

$$\partial\alpha/\partial y - (1/\chi)\partial\beta/\partial x = -2\Omega \qquad (3)$$

for all points on the blade surface.

For this analysis, the blade upper and lower surfaces are divided into curved panels as shown in Fig. 2. On each surface, there are: 19 panels of varying width in the chordwise direction; 6 panels of equal width in the spanwise direction inboard of $y/Y = 0.875$; and 6 panels of equal width in the spanwise direction outboard of this station. The half-body-of-revolution tip is divided into 6 equal-area lunes (Fig. 2) and 19 chordwise elements which match those of the airfoil section. Along the edges of these panels, the α- and β-vorticity strengths are assumed to vary linearly and to match the strengths in the adjacent panels. The α-vorticity strength is zero at the extended trailing edge. At the trailing edge, the β-vorticity filaments become trailing vortex filaments and their geometry is modified from that obtained for the lifting line as shown in Fig. 3. The trailing filaments are extended as a sheet for 10 deg of azimuth aft of the trailing edge of each panel and then are replaced by a finite strength filament. For the initial surface vorticity distribution at the tip, the α vorticity on the upper surface at (x, Y) is extended around the half-body-of-revolution tip to join with that at the same chord station on the lower surface. The strength is assumed to vary linearly over this interval to satisfy continuity.

The formation mechanism of the tip vortex is a complex phenomenon and there is little information of an experimental nature available to help define an empirical model. Although it is recognized that a viscous approach is most certainly required, several simple models were investigated to

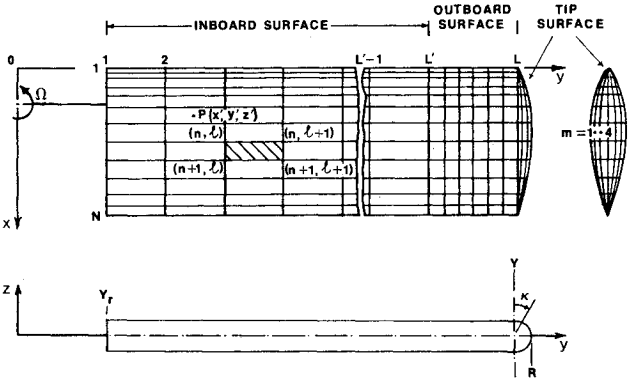

Fig. 2 Blade grid system.

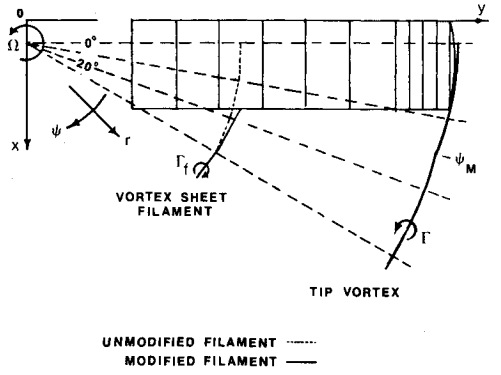

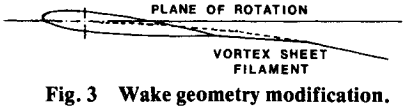

Fig. 3 Wake geometry modification.

try to give some insight into the magnitude of the problem. In each of these cases, the simple formation model is forced to join with the prescribed tip vortex geometry at azimuth, ψ_M, which is variable (Fig. 3).

One model that was tried without success was obtained by assuming that the tip vortex rolled-up off the blade trailing edge. The model was simplified by assuming that the β vorticity was shed from the blade at its trailing edge and passed along straight paths to join the tip vortex at ψ_M. The difficulty here was that convergence was not realized for the β distribution near the trailing edge.

Other models giving better results were based on the pressure distributions of Ref. 14, from which an approximate radial displacement of the tip vortex geometry could be deduced but no information on the axial displacement could be obtained. Thus, the tip vortex geometry is assumed to be given by:

$$r/RA = 1 + (B/A - 1)\exp(\lambda_M \psi) \qquad 0 \le \psi \le \psi_M \tag{4}$$

$$r/RA = 1 + (1/A - 1)\exp(\lambda \psi) \qquad \psi \ge \psi_M \tag{5}$$

$$z/RA = (1/A)k_1 \psi \qquad 0 \le \psi \le 2\pi/b \tag{6}$$

$$z/RA = (2\pi/Ab)k_1 + (1/A)k_2(\psi - 2\pi/b) \qquad \psi \ge 2\pi/b \tag{7}$$

where B and λ_M are determined by trial and error to approximately match the path of the tip vortex over the upper surface as indicated by the data of Ref. 14 and to join with the prescribed geometry at ψ_M as shown in Fig. 3. No attempt was made to join the two segments by matching the curvatures at ψ_M since this is not necessary for the numerical procedure.

The tip vortex strength is assumed to grow linearly from its assumed point of origin, (1.0082 R, 0 deg, 0), to the azimuth, ψ_S. An attempt was made to satisfy vortex continuity by joining this segment to the blade surface with geometrically simple sheets of vorticity but the several cases tried did not improve the results. Therefore, this condition is not satisfied for the final flow model. Two values of ψ_S, 5 and 10 deg, and two values of ψ_M, 15 and 20 deg, were investigated. The results showed that $\psi_S = 10$ deg (trailing edge, approximately) and $\psi_M = 15$ deg produced better overall pressure distributions.

At this point in the procedure, the complete wake geometry is specified and an initial α- and β-vorticity strength distribution has been determined. The vorticity redistribution procedure begins by using the Biot-Savart law to compute the total tangential velocity vector at the selected control points on the blade surface. The control points are at the geometric center of the panels. The Biot-Savart integral is evaluated at each control point with the integration proceeding over all of the vorticity in the field except for that surface element, ΔS, surrounding the control point. If ΔS is assumed to be planar, then the vortex sheet represented by this element cannot induce velocities tangential to itself at points in the element. Since the control point is a point in ΔS, the tangential velocity vector at the control point represents the transport velocity of ΔS as it is constrained to move along the blade surface. The vorticity vector is therefore in the plane of ΔS and perpendicular to the tangential velocity vector. Since the "fluid" within the blade surface must be at rest relative to the surface, the magnitude of the tangential velocity vector is one-half the strength of the vorticity in ΔS. Hence,

$$\tfrac{1}{2}\gamma_{\Delta S} = v_s + v_{tv} + v_{vs} + (\Omega \times r)_t \tag{8}$$

where the terms on the right-hand side are tangential components of velocity due to, respectively: the blade surface vorticity distribution, the tip vortex, the trailing vortex sheet, and the blade rotation. The flow velocity magnitude exterior and immediately adjacent to the surface sheet is

$$U = \gamma_{\Delta S} \tag{9}$$

A more complete discussion of the modeling of solid bodies by the use of vortex sheets in potential flow is given in Ref. 22.

The procedure is continued until an acceptable converged solution is obtained. Fairly good convergence is reached in three iterations although some areas of the blade require five iterations. A complete derivation of the relationships and description of the numerical procedure is given in Ref. 21. After a converged solution is obtained, the pressure distribution on the blade surface is computed by using the following equation which was obtained by integrating the momentum equation in the blade-fixed system:

$$p - p_\infty = \tfrac{1}{2}\rho\Omega^2\{[(x - 0.25)\cos\theta + z\sin\theta]^2 + y^2\} - \tfrac{1}{2}\rho U^2 \tag{10}$$

Numerical Results

The numerical analysis was developed specifically for making comparisons with the single-bladed, teetering model helicopter rotor data of Ref. 14. In operation, the blade coning angle was only a few tenths of a degree and this effect is neglected. The blade is untwisted with a constant-chord planform and a half-body of revolution tip and has an NACA 0012 airfoil section, a chord length of 12.7 cm, a tip radius, Y, of 61.0 cm, and a root radius of 15.2 cm.

Reference 21 presents chordwise pressure coefficient distributions for blade collective pitch angles of 0, 6.18, and

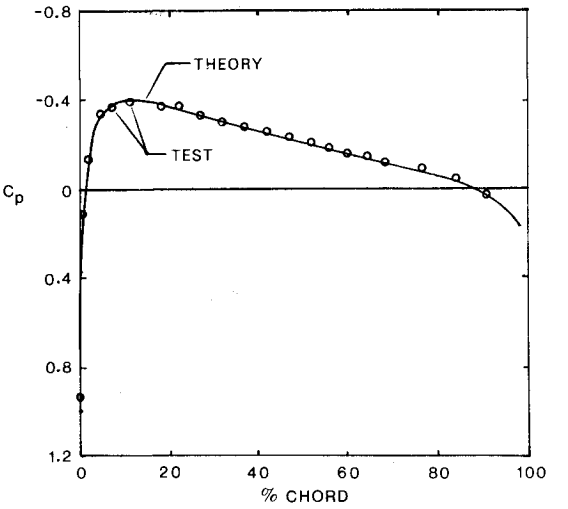

Fig. 4 Pressure coefficient distribution: $\theta = 0$ deg, $y/Y = 0.94$, $(Y-y)/c = 0.288$.

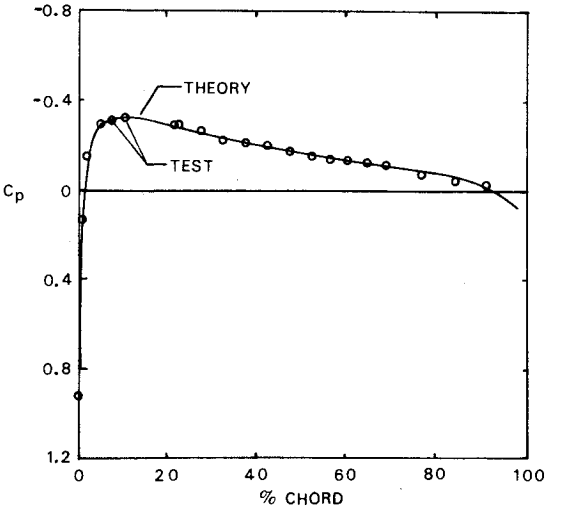

Fig. 5 Pressure coefficient distribution: $\theta = 0$ deg, $y/Y = 0.991$, $(Y-y)/c = 0.043$.

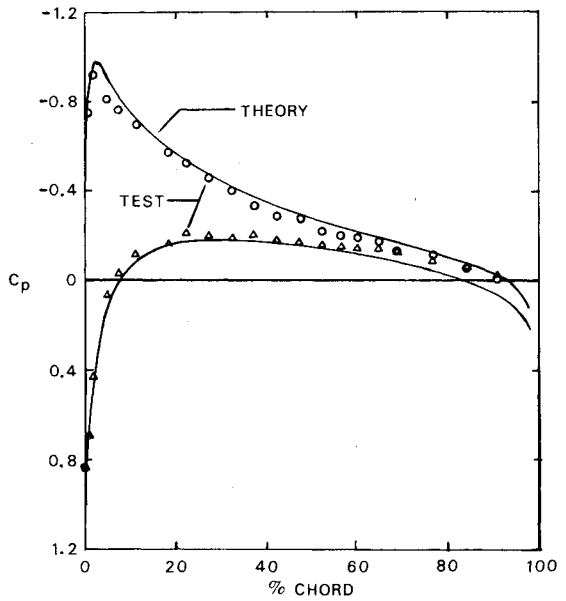

Fig. 6 Pressure coefficient distribution: $\theta = 6.18$ deg, $y/Y = 0.94$, $(Y-y)/c = 0.288$.

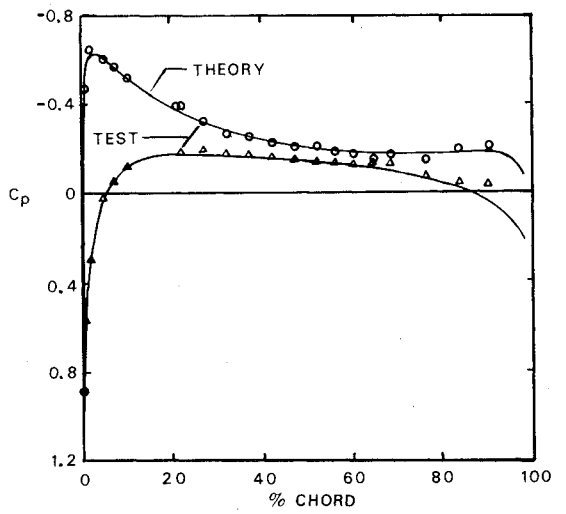

Fig. 7 Pressure coefficient distribution: $\theta = 6.18$ deg, $y/Y = 0.991$, $(Y-y)/c = 0.043$.

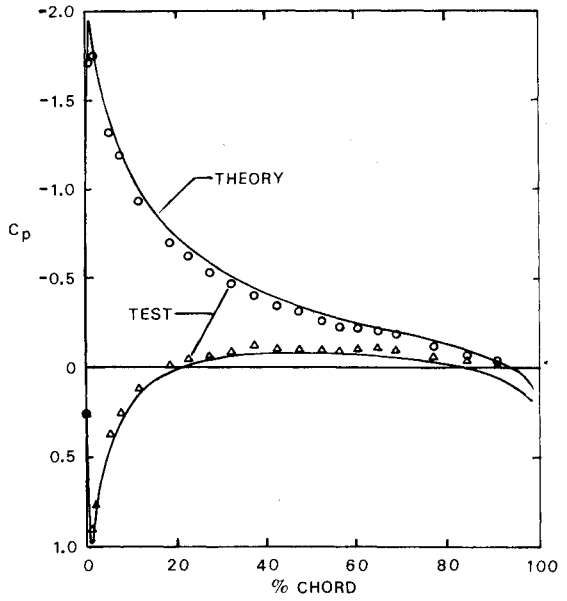

Fig. 8 Pressure coefficient distribution: $\theta = 11.4$ deg, $y/Y = 0.94$, $(Y-y)/c = 0.288$.

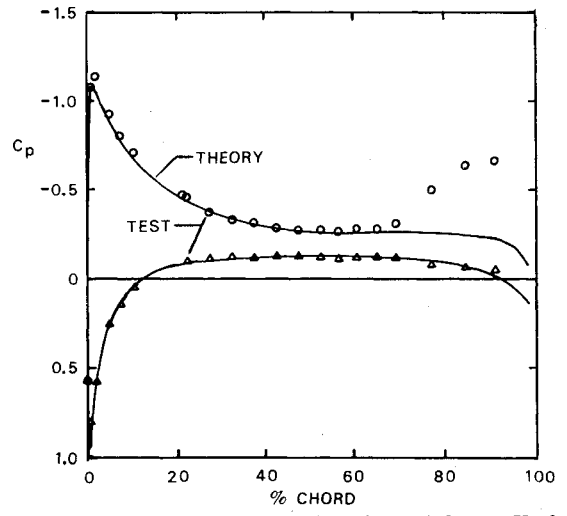

Fig. 9 Pressure coefficient distribution: $\theta = 11.4$ deg, $y/Y = 0.991$, $(Y-y)/c = 0.043$.

11.4 deg at 13 blade stations on the upper and lower surfaces and along 5 longitudes of the half-body of revolution tip. The pressure coefficients are obtained by dividing Eq. (10) by the dynamic pressure based on blade angular velocity and the section coordinate, y. Distributions of α- and β-vorticity strengths are also presented.

Typical computed pressure coefficient distributions are compared with experimental data in Figs. 4-9 for these same blade pitch angles and for blade stations at $(Y-y)/c$ of 0.288 and 0.043 or y/Y of 0.94 and 0.991, respectively. The comparison at the two stations for a blade pitch angle of 0 deg is shown in Figs. 4 and 5. The agreement over the entire surface area where data is available[14] is within experimental error. This is the nonlifting case so that there is no net trailing vorticity. The agreement is very good and it is concluded that the redistribution procedure adequately accounts for the tip-relief effect, at least in this case. Considering the very good agreement with this potential analysis, it would appear that the centrifugal pumping effect may be compensating for the chordwise boundary-layer growth effect.

The comparisons at the two stations for a blade pitch angle of 6.18 deg are shown in Figs. 6 and 7. At $y/Y = 0.94$, the potential results predict a larger normal force coefficient than that obtained from an integration of the measured distribution. Since the tip-relief and tip-vortex effects are probably small at this station and considering the good agreement for the nonlifting case, the differences shown may be due to the simple manner, Eq. (2), by which Reynolds number effect was taken into account. At $y/Y = 0.991$, the potential results agree with the measured distribution within experimental error over most of the chord length and indicates an adequate accounting for the tip-relief effect. The tip-vortex effect, though small at this station, is beginning to be observable near the trailing edge on the upper surface.

The comparisons at the two stations for a blade pitch angle of 11.4 deg are shown in Figs. 8 and 9. At $y/Y = 0.94$, the comparison is very similar to that for a blade-pitch angle of 6.18 deg. The magnitudes and locations of the positive and negative peaks near the leading edge are predicted reasonably well. At $y/Y = 0.991$, the potential results compare within experimental error on the lower surface ahead of the 91% chord and on the upper surface ahead of the 65% chord stations. Aft of the 65% chord station, the effect of the rearward sweep of the tip vortex over the upper surface becomes very strong and the analytical and experimental agreement is poor. This disagreement is attributed to the lack of an appropriate model for the formation and growth of the tip vortex. An investigation is continuing in this problem area.

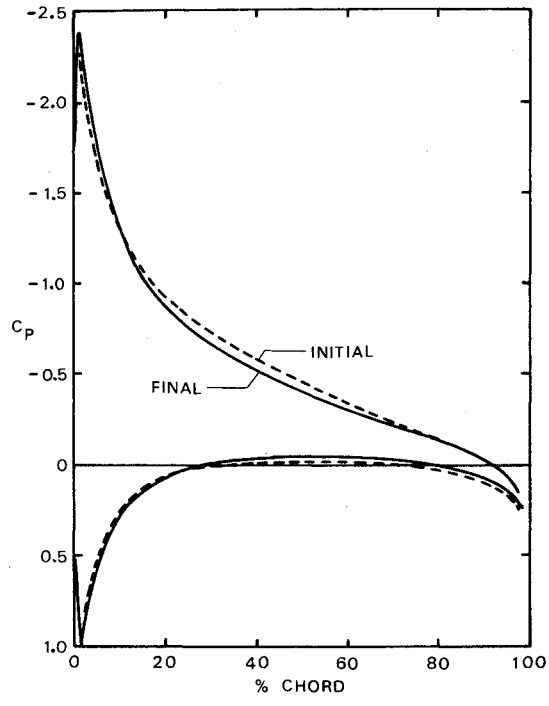

Fig. 10 Comparison of initial two-dimensional pressure coefficient distribution with that of the final iteration: $\theta = 11.4$ deg, $y/Y = 0.875$.

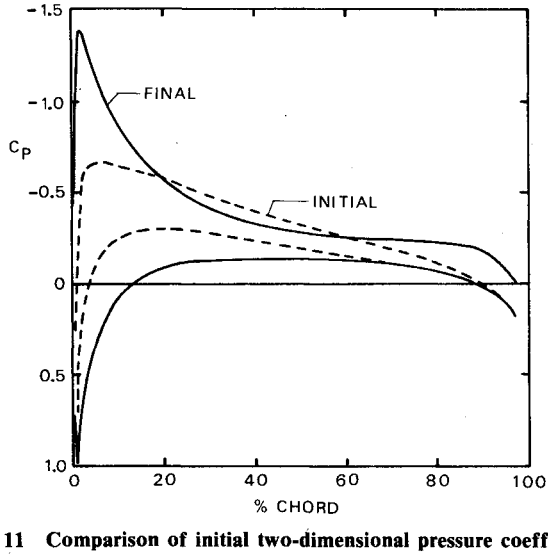

Fig. 11 Comparison of initial two-dimensional pressure coefficient distribution with that of the final iteration: $\theta = 11.4$ deg, $y/Y = 0.98$.

Figures 10 and 11 show the effect of the vorticity-redistribution procedure on the initial two-dimensional pressure coefficient distributions. Figure 10 is for $y/Y = 0.875$ and is typical for the stations inboard of that for the maximum blade bound circulation. The redistribution procedure reduces the normal force coefficient slightly and produces rather small changes in the pressure coefficient distribution. Figure 11 is for $y/Y = 0.98$ and the redistribution procedure significantly changes the initial two-dimensional distribution for those stations outboard of that for the maximum blade bound circulation.

Since the redistribution procedure iterates on the velocity component tangential to the blade surface, it is of interest to investigate how well the converged solution satisfies the boundary condition of no flow normal to the surface. For a blade pitch angle of 0 deg, the component of velocity normal to the blade surface is computed to be less than 1% of the local-blade velocity over approximately 95% of the blade area. It is greater than 1% near the leading and trailing edges but is not greater than 2% anywhere. On the half-body of revolution tip, the component is not greater than 7% of the tip speed with values this large only near the leading edge.

For a blade pitch angle of 6.18 deg, the component of velocity normal to the blade surface is computed to be less than 1% of the local blade velocity over approximately 50% of the blade area and less than 2% over approximately 90% of the blade area. Very near the blade tip, the value is as high as 6% near the leading edge and 13% near the trailing edge. On the half-body of revolution tip, the component is not greater than 13% of the tip speed with values this large only near the leading edge.

For a blade pitch angle of 11.4 deg the normal component is computed to be less than 1% of the local-blade velocity over approximately 20% of the blade area, less than 2% over approximately 60% of the blade area, and less than 3% over approximately 90% of the blade area. The value is approximately 6% very near the leading and trailing edges except at the tip where it is approximately 9%. On the half-body of revolution tip, the component is not greater than 15% of the tip speed with values this large only near the leading edge. The larger values of the normal component very near the tip are attributed to the simple modeling technique used for the tip-vortex formation.

On the CDC 6400 computer, the computational time was 6.5 min per iteration with 228 curved panels in the inboard region, 228 curved panels in the outboard region, and 114 curved panels on the half-body of revolution tip. If the geometric coefficients are stored, it is estimated that this time can be reduced to approximately 1.5 min per iteration. The time required to compute the initial two-dimensional surface vorticity distribution was 7 min. Further savings in time can be achieved by optimizing the codes.

Conclusions

The results of applying the inviscid, incompressible vorticity redistribution procedure described herein to a single-bladed hovering model rotor show the following:

1) For the nonlifting case with no net trailed vorticity, the computed pressure coefficient distribution in the tip region agrees with the measured data within experimental error over the chord length for which data are available. This agreement suggests that the neglected viscous terms generally cancel in the tip region and that the potential approach is valid in this case for investigating three-dimensional relief effects at the tip of blades having half-body of revolution tips.

2) For the lifting cases with trailed vortex sheets and strong tip vortices, the computed pressure distributions in the tip region predict the location and magnitude of the maximum and minimum pressure peaks near the leading edge to a reasonably good degree. These results suggest that the procedure accounts for the three-dimensional tip relief reasonably well in these cases.

3) For the lifting cases, the agreement between computed and measured-pressure distributions is generally good over the upper and lower surface in the tip region. However, very near the tip on the upper surface area which is strongly affected by the tip vortex, the agreement is poor. This disagreement is attributed to the lack of a proper model for the formation, growth, and rearward sweep of the tip vortex. Additional studies directed at improving this aspect of the flow model are needed.

4) Inboard of the radius of maximum bound circulation, the procedure produces rather small changes in the initial two-dimensional pressure distribution. Outboard of this radius, the changes are significant.

References

[1] Drzewiecki, S., *Bulletin de L'association technique maritime,* 1892.

[2] Reissner, H., *Zietshrift fur Mathematik,* Vol. 1, 1910.

[3]Glauert, H., "A General Theory of Autogyro," British Aeronautical Research Council, R & M No. 1111, 1926.

[4]Lock, C. N., "Application of Goldstein's Airscrew Theory to Design," British Aeronautical Research Council, R & M No. 1377, Nov. 1930.

[5]Csencsikz, T. A., Fanucci, J. B., and Chou, H. F., "Nonlinear Helicopter Rotor Lifting Surface Theory - Pt. I," West Virginia Univ., A. E. TR-35, Sept. 1973.

[6]Baskin, V. E., Vil'dgrube, L. S., Vozhdayev, Ye. S., and Maykapar,G. I., "Theory of the Lifting Airscrew," NASA TT F-823, Feb. 1976.

[7]Landgrebe, A. J., "An Analytical Method of Predicting Rotor Wake Geometry," *Journal of the American Helicopter Society,* Vol. 14, Oct. 1969, pp. 20-32.

[8]Gray, R. B. and Brown, G. W., "A Vortex Wake Analysis of a Single-Bladed Hovering Rotor and a Comparison with Experimental Data," AGARD Conf., Preprint 111 on Aerodynamics of Rotary Wings, Marseilles, France, Sept. 1972.

[9]Gray, R. B., "On the Motion of the Helical Vortex Shed from a Single-Bladed Hovering Model Helicopter Rotor and its Application to the Calculation of the Spanwise Aerodynamic Loading," Princeton Univ. Aero. Engr. Dept., Rept. No. 313, Sept. 1955.

[10]Gray, R. B., "An Aerodynamic Analysis of a Single-Bladed Rotor in Hover and in Low-Speed Forward Flight as Determined from Smoke Studies of the Vorticity Distribution in the Wake," Princeton Univ., Aero. Engr. Dept., Rept. No. 356, 1956.

[11]Landgrebe, A. J., "The Wake Geometry of a Hovering Helicopter Rotor and Its Influence on Rotor Performance," *Journal of the American Helicopter Society,* Vol. 17, Oct. 1972, pp. 3-15.

[12]Kocurek, J. D. and Tangler, J. L., "A Prescribed Wake Lifting Surface Hover Performance Analysis," *Journal of the American Helicopter Society,* Vol. 22, Jan. 1977, pp. 24-35.

[13]Shivananda, T. P., McMahon, H. M., and Gray, R. B., "Surface Pressure Measurements at the Tip of a Model Helicopter Rotor in Hover," *Journal of Aircraft,* Vol. 15, Aug. 1978, pp. 460-467.

[14]Gray, R. B., McMahon, H. M., Shenoy, K. R., and Hammer, M. L., "Surface Pressure Measurements at Two Tips of a Model Helicopter Rotor in Hover," NASA CR 3281, May 1980.

[15]Preuss, R. D., Suciu, E. O., and Morino, L., "Unsteady Potential Aerodynamics of Rotors with Applications to Horizontal-Axis Windmills," *AIAA Journal,* Vol. 18, April 1980, pp. 385-393.

[16]Soohoo, P., Noll, R. B., Morino, L., and Ham, N. D., "Green's Function Method for the Computational Aerodynamic Analysis of Complex Helicopter Configurations," AIAA Paper 79-0347, New Orleans, La., Jan. 1979.

[17]Samant, S. S. and Gray, R. B., "A Semi-Empirical Correction for the Vortex Core Effect on Hovering Rotor Wake Geometries," *Proceedings of the 33rd Annual National Forum of the American Helicopter Society,* May 1977, pp.02-1-02-10.

[18]Landgrebe, A. J., Moffitt, R. C., and Clark, D. R., "Aerodynamic Technology for Advanced Rotorcraft-Part I," *Journal of the American Helicopter Society,* Vol. 22, April 1977, pp. 21-27.

[19]Kocurek, J. D., Berkowitz, L. F., and Harris, F. D., "Hover Performance Methodology at Bell Helicopter Textron," *Proceedings of the 36th Annual National Forum of the American Helicopter Society,* May 1980, pp. 3-1-3-47.

[20]Raj, P. and Gray, R. B., "Computation of Three-Dimensional Potential Flow Using Surface Vorticity Distribution," *Journal of Aircraft,* Vol. 16, March 1979, pp. 162-169.

[21]Shenoy, K. R., "A Method of Computing the Pressure Distribution on a Single-Bladed Hovering Helicopter Rotor," Ph.D. Dissertation, Georgia Inst. of Tech., Jan. 1979. (Available from University Microfilms International.)

[22]von Mises, R., *Theory of Flight,* 1st ed., McGraw Hill, N. Y., 1945, pp. 188-198, 211-231.

From the AIAA Progress in Astronautics and Aeronautics Series . . .

INSTRUMENTATION FOR AIRBREATHING PROPULSION—v. 34

Edited by Allen Fuhs, Naval Postgraduate School, and Marshall Kingery, Arnold Engineering Development Center

This volume presents thirty-nine studies in advanced instrumentation for turbojet engines, covering measurement and monitoring of internal inlet flow, compressor internal aerodynamics, turbojet, ramjet, and composite combustors, turbines, propulsion controls, and engine condition monitoring. Includes applications of techniques of holography, laser velocimetry, Raman scattering, fluorescence, and ultrasonics, in addition to refinements of existing techniques.

Both inflight and research instrumentation requirements are considered in evaluating what to measure and how to measure it. Critical new parameters for engine controls must be measured with improved instrumentation. Inlet flow monitoring covers transducers, test requirements, dynamic distortion, and advanced instrumentation applications. Compressor studies examine both basic phenomena and dynamic flow, with special monitoring parameters.

Combustor applications review the state-of-the-art, proposing flowfield diagnosis and holography to monitor jets, nozzles, droplets, sprays, and particle combustion. Turbine monitoring, propulsion control sensing and pyrometry, and total engine condition monitoring, with cost factors, conclude the coverage.

547 pp. 6 x 9, illus. $14.00 Mem. $20.00 List

TO ORDER WRITE: Publications Dept., AIAA, 1290 Avenue of the Americas, New York, N. Y. 10019